Journal Name

ARTICLE

Photoelectrochemical manifestation of intrinsic photoelectron transport properties of vertically aligned {001} faceted single crystal TiO_2 nanosheet films

Received 00th January 20xx,
Accepted 00th January 20xx

DOI: 10.1039/x0xx00000x

www.rsc.org/

Yang Lu,[a] Guozhong Wang,[a] Haimin Zhang,[*a] Yunxia Zhang,[a] Shenghong Kang[a] and Huijun Zhao[*ab]

In this work, vertically aligned anatase TiO_2 single crystal nanosheets with laterally exposed {001} facets onto conducting FTO substrate (VATN) were successfully synthesised using hydrofluoric acid (40 wt%) as crystal facet controlling agent by a simple hydrothermal method. The as-synthesised VATN wihtout calcination exhibited good crystalline structure, and was used as photoanode showing superior photoelectrocatalytic activity toward water oxidation under UV irradiation. After thermal treatment at 550 °C for 2 h, the photoelectrocatalytic activity of VATN photoanode was almost 2.6 times of that for unsintered VATN under the same experimental conditions, which could be mainly due to surface passivation role of surface fluorine in unsintered VATN to decrease photoelectrocatalytic activity. A photoelectrochemical method was used to manifest the photoelectron transport properties inside VATN photoanodes and concurrently quantify the inherent resistances (R_0) of UV illuminated photoanodes before and after calcination. The results demonstrated that the determined R_0 values were respectively 155 Ω and 66 Ω for VATN photoanodes before and after calcination, inversely proportional to their photoelectrocatalytic activities. Compared to VATN before calcination, significantly decreased R_0 value of VATN after calcination further confirmed the presence of surface fluorine in VATN unfavorable for photoelectron transport inside photocatalyst film. This work provided a direct evidence to prove the intrinsic photoelectron transport properties of {001} faceted anatase TiO_2 nanosheet array film photoanodes at the presence and absence of surface fluorine.

1. Introduction

Nanostructured titanium dioxides (TiO_2) have been the most extensively investigated semiconductor materials due to their importance in environment, energy, biomedicine and sensing applications.[1-4] A recent discovery of performance dependence on crystal facets of TiO_2 nanocrystals has stimulated a new upsurge interest to synthesise nanostructured TiO_2 crystals with various high energy facets.[5] To date, the anatase TiO_2 crystals with exposed {001} facets are the most widely investigated high energy faceted TiO_2 nanocrystals due to their superior photocatalytic properties.[5-12] It has been well demonstrated that in comparison to anatase TiO_2 nanocrystals with exposed {101} facets, the {001} faceted nanocrystals possess superior photocatalytic and photoelectrocatalytic activities toward oxidative decomposition of water and organic pollutants.[9-11] Theoretical studies have indicated that the superior photocatalytic activity of {001} faceted anatase TiO_2 nanocrystals can be attributed largely to their high surface energy (0.90 J m^{-2}), which is more than double of that for {101} facets (0.44 J m^{-2}).[8, 12, 13] However, fundamental photocatalysis processes such as surface adsorption and electron transfer processes that are important in determining the photocatalytic activity and directly related to the exposed crystal facets of photocatalysts have not yet been quantitatively investigated. This is due partially to the fact that the vast majority of {001} faceted anatase TiO_2 nanocrystals are synthesised in powder forms and used in solution suspension systems for photocatalysis applications for which quantitative determination of adsorption and electron transfer properties of photocatalysts is difficult because of complexity involved.[5, 6, 14-17] Recently, we and others have demonstrated that {001} faceted anatase TiO_2 nanocrystals can be directly grown onto conducting substrate such as FTO glass.[11, 18-28] The immobilisation of photocatalysts onto conducting substrates allows the application of photoelectrochemical techniques that are advantageous for quantitative investigation of interfacial photocatalysis processes and electron migration process inside of photocatalysts.[14-17, 29-31] We recently demonstrated that the adsorption properties (*e.g.*, adsorption constant and maximum adsorption capacity) of oxalic acid at the surface of a {001} faceted anatase TiO_2 photoanode can be facilely quantified by a photoelectrocatalytic method.[28] It is well known that the photocatalytic activity of a photocatalyst is highly dependent on the separation efficiency of photogenerated electrons and holes. The superior charge separation ability could be an important factor responsible for the superior photocatalytic activity

[a] *Key Laboratory of Materials Physics, Centre for Environmental and Energy Nanomaterials, Anhui Key Laboratory of Nanomaterials and Nanotechnology, Institute of Solid State Physics, Chinese Academy of Sciences, Hefei 230031, China. E-mail: zhanghm@issp.ac.cn*
[b] *Centre for Clean Environment and Energy, Gold Coast Campus, Griffith University, Queensland 4222, Australia. E-mail: h.zhao@griffith.edu.cn*

obtained from high energy faceted anatase TiO_2 nanocrystals, which can be directly reflected by the photoelectron transport capability inside of photocatalysts.[14, 29-31] Therefore, it is of a scientific interest to gain insightful knowledge on the intrinsic photoelectron transport properties of {001} faceted anatase TiO_2 photocatalysts. In this regard, we have previously demonstrated that the photoelectron transport properties can be manifested by the photoelectrocatalytically determined intrinsic photocatalytic resistance (R_0) inside the photocatalysts.[14, 29-31]

Herein, photoanodes are purposely fabricated by directly hydrothermal growth of vertically aligned anatase TiO_2 single crystal nanosheets with laterally exposed {001} facets onto conducting FTO substrate (VATN). The intrinsic photoelectron transport resistance inside the as-synthesised and the thermally treated VATN photoanodes are quantitatively determined by a facile photoelectrocatalytic method.[14, 29-31] Although the as-synthesised VATN possesses similar crystallinity as that of the thermally treated, the later exhibits a significantly improved photoelectrocatalytic activity toward water oxidation due to the low intrinsic photoelectron transport resistance resulting from the complete removal of surface fluorine under high temperature treatment conditions. Interestingly, the determined photoelectrocatalytic activities from these photoanodes are found to be inversely proportional to their intrinsic resistance, suggesting that the photocatalytic activity of a photocatalyst can be facilely quantified by quantifying the intrinsic photoelectron transport properties inside the photocatalyst.

2. Experimental section

2.1 Synthesis

To grow vertically aligned anatase TiO_2 crystal nanosheets film (VATN), a 5.0 nm thickness amorphous TiO_2 layer was firstly deposited on cleaned fluorine doped tin oxide (FTO) glass substrate (7 Ω/□, 30 mm × 15 mm × 2 mm) by the atomic layer deposition technique, and followed by annealing at 550 °C for 30 min in air for crystallisation. Subsequently, a mixed reaction solution was prepared as follows: 0.5 mL of $Ti(OBu)_4$ (98 wt%) was added slowly into a solution containing18 mL of HCl (6.0 M) and 1.0 mL of H_2O_2 (30 wt%), under magnetic stirring in a Teflon vessel (30 mL in volume). After 20 min, 180 μL of HF (40 wt%) was added into the above solution for another 5 min stirring. In this work, HF was used as crystal facet controlling agent to effectively decrease the surface energy of anatase TiO_2 {001} facets with a high surface energy of 0.90 J/m^2 by surface fluorination, thus synthesising {001} faceted TiO_2 nanosheets.[12] Before hydrothermal reaction, a pretreated FTO substrate with anatase TiO_2 compact layer was placed into the Teflon vessel with conductive side facing up. Then, the Teflon vessel was sealed in a stainless steel autoclave, and heated up to 160 °C for 20 h. After hydrothermal reaction, the autoclave was cooled quickly down to room temperature. The obtained sample was cleaned in an ethanol aqueous solution (1:1, v/v) using an ultrasonic bath for 10 min, and then adequately rinsed with deionised water. The as-synthesised TiO_2 film was also calcined in muffle furnace at 550 °C for 2 h in air to completely remove surface fluorine.

2.2 Characterisation

The structure of the as-prepared anatase TiO_2naonsheet array films were investigated by using an X-ray diffraction (X'Pert Pro MPD) with Cu Kα radiation (λ=1.54056 Å). The morphological properties of samples were characterised by field-emission scanning electron microscopy (FESEM; Hitachi SU8020). The microstructures were analysed by TEM instruments (JEM-2010, 200 kV). For TEM sample preparation, VATN samples were scrapped from FTO substrates, and dispersed in water under ultrasonic. The elemental composition of VATN samples was measured with XPS spectrometer (Thermo ESCALAB 250) with Al Kα X-ray as the excitation source and all the XPS spectra were calibrated by the C1s signal to the binding energy of 284.6 eV.

2.3 Photoelectrochemical measurements

The photoelectrochemical measurements were performed through a photoelectrochemical cell with a quartz window for illumination.[15, 32] A three-electrode mode, consisting of a VATN photoanode, a saturated Ag/AgCl reference electrode and a platinum mesh counter electrode, was applied in the experiments. A 0.10 M $NaNO_3$ aqueous solution at pH 7.0 was used as electrolyte in the measurements. An electrochemical workstation (CHI760E Instruments) was used for the application of potential bias. The irradiating light was 365 nm parallel ultraviolet from a 350 W Xe arc lamp light source fitted with focusing lenses, UV band pass filter (Wavelength < 400 nm), and 365 nm band pass filter (CHF-XM-350W, Beijing Trusttech Co. Ltd., China). The light intensity at 365 nm was carefully measured with a UV irradiance meter equipped with UV365 detector (UV-A, Instruments of Beijing Normal University, China).

3. Results and discussion

3.1 Structure and composition

The crystallographic structure of vertically aligned anatase TiO_2 crystal nanosheets film (VATN) before and after calcination at 550 °C for 2 h was firstly confirmed by X-ray diffraction (XRD) technique as shown in Fig. 1. It was found that the VATN before and after calcination show good and similar crystalline structure which is tetragonal anatase TiO_2 with a space group of $I4_1/amd$ (JCPDS No. 21-1272).[33] Due to good crystalline nature, the VATN photoanode without calcination may possess good photoelectrocatalytic activity.

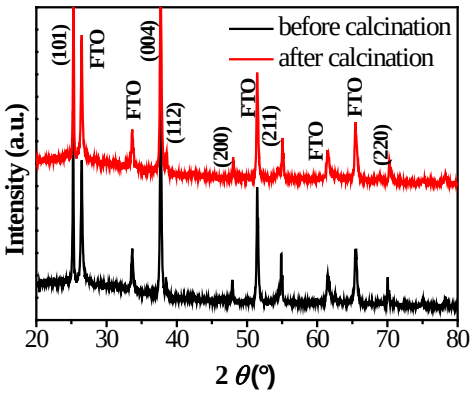

Fig. 1 XRD patterns of VATN before and after calcination at 550 °C.

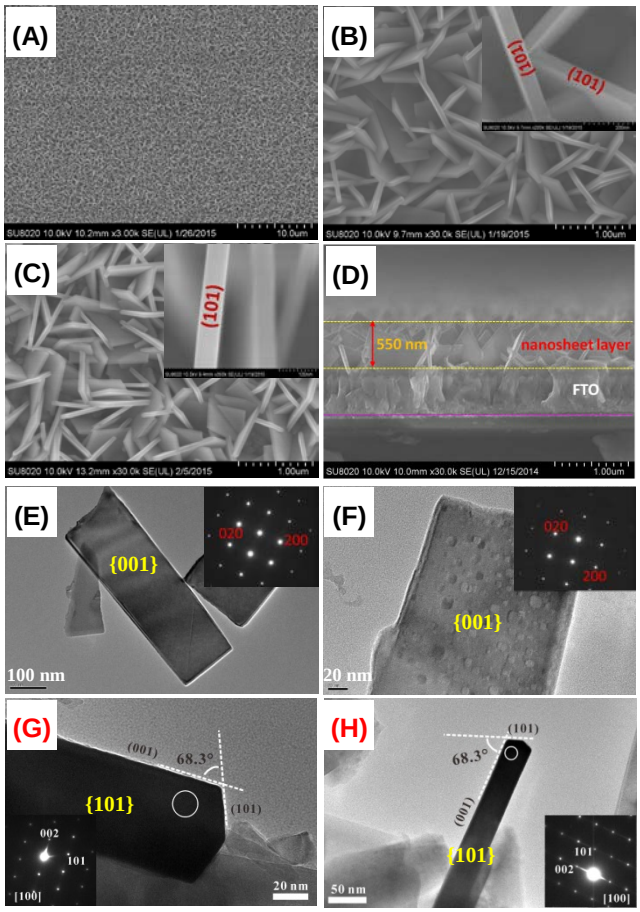

Fig. 2(A, B) Low and high magnification surface SEM images of {001} faceted anatase TiO_2 films before calcination. (C) Surface SEM image of {001} faceted anatase TiO_2 film after calcination. (D) Cross-sectional SEM image of {001} faceted anatase TiO_2 film after calcination. (E, F) TEM images of {001} facet exposed anatase nanosheets before and after calcination; the insets of corresponding SAED patterns. (G, H) TEM images of {101} facet exposed anatase nanosheets before and after calcination; the insets of corresponding SAED patterns.

Fig. 2 shows the SEM and TEM images of VATN before and after calcination. As shown, the as-synthesised VATN without calcination exhibits very uniform film structure (Fig. 2A). The high magnification SEM image (Fig. 2B) demonstrates the detailed film structure composed of vertically aligned TiO_2 nanosheets with top exposed (101) surface and lateral large (001) surface (Fig. 2E). After calcination, a similar film structure can be observed (Fig. 2C), indicating high thermal stability of the fabricated anatase nanosheets. The obtained nanosheets before and after calcination possess *ca.* 50 nm in thickness (insets in Fig. 2B and C), vertically grown onto FTO substrate. This was further evidenced by the cross-sectional SEM image (Fig. 2D). As shown, the VATN displays a thickness of *ca.*550 nm, and composed of vertically aligned nanosheets. This nanosheet array structure may be favourable for photoelectron transport inside photocatalyst film, thus significantly decreasing the recombination of photogenerated carriers and improving the photoelectrocatalytic activity. TEM characterisation demonstrates that the obtained nanosheets without calcination display very smooth lateral surfaces (Fig. 2E), while a rough surface with cavity structures can be clearly observed for the calcined sample (Fig. 2F).

However, it is still unclear for the produced reason of these cavities on anatase (001) surface. Some studies have suggested that these cavities on anatase (001) surface may be due to substantial F^- etching or Ti-OH removal in crystal lattices during high temperature thermal treatment.[20,34-36] Further, the SAED patterns (insets in Fig. 2E and F) of anatase TiO_2 nanosheets before and after calcination reveal good single crystal nature of the nanosheet with lateral (001) surface.[8-12] Moreover, further TEM images and SAED patterns (Fig. 2G, H) confirm the top exposed surface of (101) surface of anatase nanosheets before and after calcination (Fig. 2B, C).[12] The high crystalline nanosheets with good arrayed structure property may be favourable for improving photoelectron transport capability and photoelectrocatalytic performance when used as photoanode.

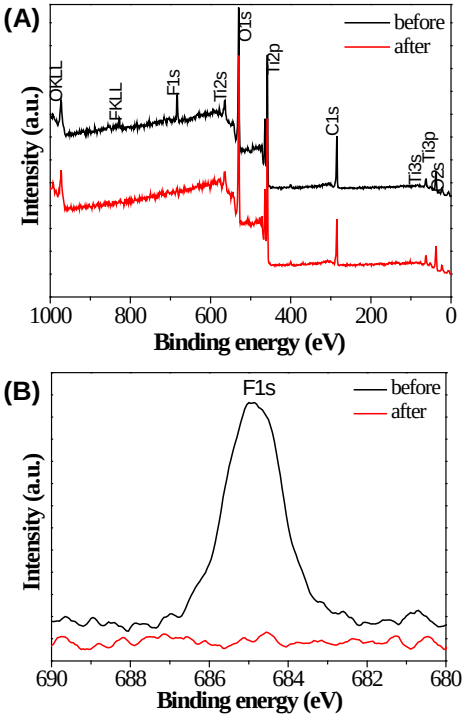

Fig. 3 (A) Surface survey XPS spectra of {001} faceted anatase TiO_2 nanosheet films before and after calcination. (B) High-resolution XPS spectra of F1s of {001} faceted anatase TiO_2 nanosheet films before and after calcination.

In this work, the element composition of VATN samples before and after calcination was investigated by X-ray photoelectron spectra (XPS). Fig. 3A shows the surface survey XPS spectra of VATN samples before and after calcination. As shown, the F1s peak, as well as those of Ti, O, and C, is clearly observed for VATN sample before calcination, while fluorine element is completely disappeared for the calcined sample. This can be further evidenced by high-resolution XPS spectra. As shown in Fig. 3B, the F1s peak is clearly visible at about 685.0 eV for VATN before calcination owing to fluorinated TiO_2 system such as ≡Ti-F species on the TiO_2 crystal surface by hydrothermal reaction,[12, 37, 38] while no fluorine element was detected after calcination, indicating fluorine element completely disappeared after calcination at 550 °C for 2 h. Furthermore, no fluorine ions in the crystal lattice (bonding energy of *ca.* 688.0-689.0 eV) were observed, implying the oxygen in TiO_2

lattice was not substituted by fluorine.[12, 37, 38] Many studies have demonstrated that although surface fluorination plays a crucial role in the formation of {001} faceted TiO_2 nanocrystals, the presence of surface fluorine is very disadvantageous for improving photocatalytic activity.[12, 33, 39] In reported studies, high temperature thermal treatment is generally adopted to completely remove surface fluorine and improve photocatalytic performance of {001} faceted anatase TiO_2 nanocrystal photocatalysts.[12, 33, 39] The influencing origin of surface fluorine on photocatalytic activity is still unclear, which deserves an in-depth investigation (*e.g.*, the influence of surface fluorine on photoelectron transport of {001} faceted anatase TiO_2 nanocrystals).

3.2 Photoelectrocatalytic activities

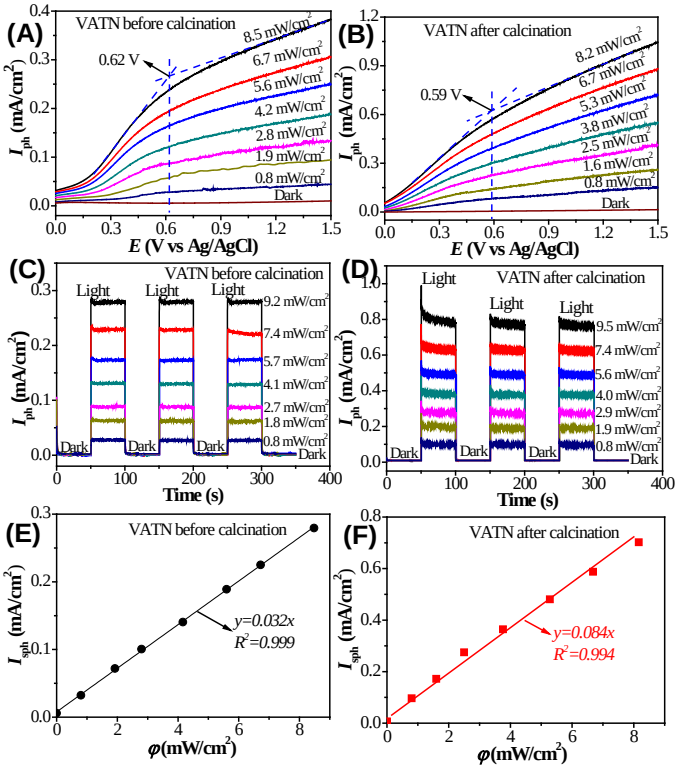

Fig. 4 (A) and (B) Voltammograms obtained from VATN photoanodes before and after calcination in 0.10 M $NaNO_3$ electrolyte under different UV intensities. (C) and (D) Transient photocurrent responses obtained at +0.80 V applied potential bias with different UV intensities for VATN photoanodes before and after calcination. (E) and (F) I_{sph}-φ relationships derived from Fig. 4A and B.

{001} faceted anatase TiO_2 nanocrystals have been widely investigated as photocatalysts for photocatalytic degradation of organic pollutants.[5, 6] However, the report is few using {001} faceted anatase TiO_2 nanocrystals for photoelectrocatalytic application. Very recently, Yang and co-workers fabricated {001} faceted hierarchical TiO_2 nanoflowers/nanosheets array film.[25] After sensitisation with CdS quantum dots, the {001} faceted TiO_2 nanoflowers/nanosheets array film as photoanode exhibited superior photoelectrocatalytic activity under sunlight irradiation. In this work, the VATN samples before and after calcination were also evaluated as photoanodes for photoelectrocatalytic oxidation of water under UV irradiation. Fig. 4A and B show the voltammograms of VATN photoanodes before and after calcination in 0.10 M $NaNO_3$ electrolyte under different UV irradiation intensities. It was found that the VATN without calcination can be directly used as photoanode, exhibiting good photoelectrocatalytic activity toward water oxidation (Fig. 4A). It can be seen from Fig. 4A and B that without UV irradiation, only a negligible dark current can be observed. For all cases under UV irradiation, the measured photocurrents were found to be linearly increased with applied potential bias within the low potential range (*e.g.*, within 0.62 V and 0.59 V for VATN photoanodes before and after calcination). Our previous studies have revealed that the linearly increased photocurrent can be ascribed to the limitation of free photoelectron transport inside TiO_2 photocatalyst film.[14, 17, 29] At higher potentials, the photocurrents tend to be saturated owing to the limitation of the interfacial processes at TiO_2 catalyst/electrolyte interface.[14, 17, 29] Clearly, an increase in the light intensity leads to an increase in the saturation photocurrents (I_{sph}) for all investigated photoanodes.

The transient photocurrent response curves of all investigated photoanodes further confirm this as shown in Fig. 4C and D. Moreover, all photoelectrochemical measurement results demonstrate that for a given UV intensity (φ), the saturation photocurrent (I_{sph}) of VATN after calcination is obviously higher than that of VATN before calcination, indicating superior photoelectrocatalytic activity of the calcined photoanode. Fig. 4E and F show the plots of saturation photocurrents(I_{sph}) derived from Fig. 4A and B at +0.8 V against UV intensities (φ) for VATN photoanodes before and after calcination. Linear relationships can be obtained for all investigated photoanodes, showing slope values of 0.032 mA/mW (R^2 = 0.999) and 0.084 mA/mW (R^2 = 0.994) for VATN photoanodes before and after calcination under UV irradiation, respectively. Under the given experimental conditions, the slope value represents the photoelectrocatalytic activity of the investigated photoanode.[9, 40] Apparently, the slope value of VATN photoanode after calcination is almost 2.6 times of unsintered photoanode, indicating higher photoelectrocatalytic activity toward water oxidation. This improved photoelectrocatalytic performance of VATN after calcination could be due to the complete removal of surface fluorine of anatase TiO_2 nanosheets and enhanced crystallinity of VATN decreasing crystal defects etc., favourable for photoelectron transport inside VATN film.[20, 34, 39] Considering similar crystalline structure of VATN before and after calcination, the complete removal of surface fluorine may play more important role in improving the photoelectron transport capability, thus photoelectrocatalytic activity of VATN.

3.3 Photoelectron transport properties

Our previous works have demonstrated that the photoelectron transport process inside a photocatalyst film can be quantitatively manifested by the photoelectron transport resistance (namely, intrinsic photocatalyst resistance, R_0) using a simple and effective photoelectrocatalytic method.[14, 29-31] In this work, the R_0 values of VATN photoanodes before and after calcination were also determined by this developed photoelectrocatalytic method. From Fig. 4A and B, the I_{ph}-E curves reveal a linear photocurrent increase with applied potential bias within low potential range for each given UV intensity. The linear part of I_{ph}-E curve indicates a pure resistor-type behaviour, implying that the overall reaction is controlled by

the photoelectron transport process inside the photocatalyst film.[14, 29-31] Under such conditions, the rapidity of the photoelectron transport across the photocatalyst film will determine the rate of the overall reaction.[14, 29-31] Based on this developed method,[14, 29-31] the overall resistance (R) value of each voltammogram from Fig. 4A and B for VATN photoanodes before and after calcination under UV irradiation can be calculated. Further, plotting R values against saturation photocurrent values (I_{sph}) obtained from Fig. 4A and B gives hyperbolic curves as shown in Fig. 5A and B for VATN photoanodes before and after calcination under UV irradiation, respectively. The relationship between R and I_{sph} can be expressed as below equation:

$$R = k/I_{sph} + R_0 = R_I + R_0$$

where k is a proportionality constant; I_{sph} is the saturation photocurrent; R_0 and R_I are the constant and the variant components of the resistance, respectively.

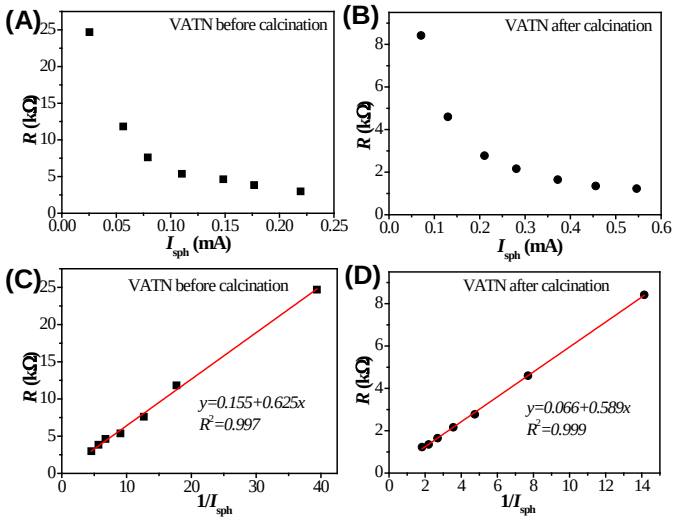

Fig. 5 (A) and (B) Relationships between the measured resistance and saturation photocurrent of VATN photoanodes before and after calcination under UV irradiation. (C) and (D) Relationships between the resistance and inversed saturation photocurrent of VATN photoanodes before and after calcination under UV irradiation. Data were derived from Fig. 4A and B.

Table 1 The calculated k and R_0 values of different TiO_2 nanostructure films reported in literatures and current work.

Photoanodes	Film thickness (μm)	k (Ω mA)	R_0 (Ω)
Anatase TiO_2 nanoparticle film[14]	1	364	245
Anatase TiO_2 nanotube film[29, 30]	0.256	613	51.0
	0.87	525	71.0
Rutile TiO_2 nanowire bundle film[30]	0.9	592	52.1
{111} faceted Rutile TiO_2 film[31]	5.0	315	93.5
VATN film before calcination	0.55	625	155
VATN film after calcination	0.55	589	66

Previous studies reported by our group have indicated that the constant component, R_0, collectively represents the TiO_2 crystal boundary resistances and the resistances at TiO_2/conducting substrate interface, which is an intrinsic property of the photoanode, independent of experimental conditions.[14, 29-31] Fig. 5C and D show the curves of R values against $1/I_{sph}$ values for VATN photoanodes before and after calcination, exhibiting good linear relationships. From Fig. 5C and D, R_0 values obtained from the intercepts of R–$1/I_{sph}$ curves are 155 Ω and 66 Ω for VATN photoanodes before and after calcination, respectively. Obviously, the VATN photoanode after calcination possesses smaller R_0 value compared to unsintered VATN, indicating superior photoelectron transport capability. After calcination, the complete removal of surface fluorine of VATN may be favourable for the photoelectron transport inside photocatalyst film, thus resulting in higher photoelectrocatalytic activity. Interestingly, it was found that the determined photoelectrocatalytic activities from these two photoanodes (the photoelectrocatalytic activity of thermally treated VATN is almost 2.6 times of that of unsintered VATN) are essentially inverse proportional to their intrinsic resistances (the R_0 value of unsintered VATN is about 2.4 times of that for sintered VATN), implying that the photocatalytic activity of a photocatalyst can be facilely quantified by quantifying the intrinsic photoelectron transport properties inside the photocatalyst. Our previous work has clarified that the proportionality constant, k, can be interpreted as the minimum applied potential bias required to remove 100% of the photoelectrons from the photocatalyst film.[29-31] The magnitude of k value manifests the readiness of the photoelectron removal in the photocatalyst film.[29-31] After calcination, the k value of VATN is 30 mV less than that of VATN before calcination, indicating the photoelectron removal is much easier from VATN owing to the superior photoelectron transport capability after complete removal of surface fluorine. Considering the same experimental conditions and the VATN samples with similar crystalline structure before and after calcination, surface fluorine may have important influence on the photoelectron transport property inside photocatalyst film, thus affecting the photoelectrocatalytic activity of VATN photoanode. Compared to other TiO_2 nanostructure array films reported in literatures,[29-31] the {001} faceted anatase TiO_2 nanosheet array film after calcination exhibits comparable R_0 value, further verifying its superior photoelectron transport property owing to good single crystal nature.

4. Conclusions

In summary, vertically aligned anatase TiO_2 nanosheets with laterally exposed {001} facets films (VATN) were synthesised onto conducting FTO substrates by a simple hydrothermal method. Owing to high crystallinity, the as-synthesised VATN without calcination can be directly used as photoanode for photoelectrocatalytic oxidation of water, exhibiting superior photoelectrocatalytic activity. After complete removal of surface fluorine at 550 °C for 2 h, VATN photoanode showed significantly improved photoelectrocatalytic performance toward water oxidation. This improved photoelectrocatalytic activity can be ascribed to the superior photoelectron transport

property of VATN photoanode after calcination, which has been verified by the calculated photoelectron transport resistance (R_0) by a simple photoelectrochemical method. Our study demonstrated that the presence of surface fluorine in VATN could be unfavourable for the photoelectron transport inside photocatalyst film, thus resulting in low photoelectrocatalytic activity. Additionally, this photoelectrochemical method would be a simple and effective tool to quantitatively characterise the intrinsic photoelectron transport properties of other semiconductor photocatalysts.

Acknowledgements

This work was financially supported by the National Natural Science Foundation of China (Grant No. 51072199, 51372248 and 51272255), the Hundred Talent Program of the Chinese Academy of Sciences and CAS/SAFEA International Partnership Program for Creative Research Teams of Chinese Academy of Sciences, China.

References

1. A. L. Linsebigler, G. Q. Lu and J. T. Yates, *Chem Rev*, 1995, **95**, 735-758.
2. M. Gratzel, *Nature*, 2001, **414**, 338-344.
3. U. Diebold, *Surface Science Reports*, 2003, **48**, 53-229.
4. X. Chen and S. S. Mao, *Chem Rev*, 2007, **107**, 2891-2959.
5. G. Liu, H. G. Yang, J. Pan, Y. Q. Yang, G. Q. Lu and H. M. Cheng, *Chem Rev*, 2014, **114**, 9559-9612.
6. W. J. Ong, L. L. Tan, S. P. Chai, S. T. Yong and A. R. Mohamed, *Nanoscale*, 2014, **6**, 1946-2008.
7. M. Kapilashrami, Y. F. Zhang, Y. S. Liu, A. Hagfeldt and J. H. Guo, *Chem Rev*, 2014, **114**, 9662-9707.
8. Y. Wang, H. M. Zhang, Y. H. Han, P. R. Liu, X. D. Yao and H. J. Zhao, *Chem Commun*, 2011, **47**, 2829-2831.
9. H. M. Zhang, P. R. Liu, F. Li, H. W. Liu, Y. Wang, S. Q. Zhang, M. X. Guo, H. M. Cheng and H. J. Zhao, *Chem-Eur J*, 2011, **17**, 5949-5957.
10. H. M. Zhang, Y. Wang, P. R. Liu, Y. H. Han, X. D. Yao, J. Zou, H. M. Cheng and H. J. Zhao, *Acs Appl Mater Inter*, 2011, **3**, 2472-2478.
11. P. R. Liu, Y. Wang, H. M. Zhang, T. C. An, H. G. Yang, Z. Y. Tang, W. P. Cai and H. J. Zhao, *Small*, 2012, **8**, 3664-3673.
12. H. G. Yang, C. H. Sun, S. Z. Qiao, J. Zou, G. Liu, S. C. Smith, H. M. Cheng and G. Q. Lu, *Nature*, 2008, **453**, 638-U634.
13. Y. Wang, H. M. Zhang, P. R. Liu, T. Sun, Y. B. Li, H. G. Yang, X. D. Yao and H. J. Zhao, *J Mater Chem A*, 2013, **1**, 12948-12953.
14. D. L. Jiang, H. J. Zhao, S. Q. Zhang and R. John, *J Phys Chem B*, 2003, **107**, 12774-12780.
15. D. L. Jiang, H. J. Zhao, S. Q. Zhang, R. John and G. D. Will, *J Photoch Photobio A*, 2003, **156**, 201-206.
16. D. L. Jiang, H. J. Zhao, S. Q. Zhang and R. John, *J Catal*, 2004, **223**, 212-220.
17. D. L. Jiang, S. Q. Zhang and H. J. Zhao, *Environ Sci Technol*, 2007, **41**, 303-308.
18. S. L. Feng, J. Y. Yang, H. Zhu, M. Liu, J. S. Zhang, J. Wu and J. Y. Wan, *J Am Ceram Soc*, 2011, **94**, 310-315.
19. W. X. Guo, F. Zhang, C. J. Lin and Z. L. Wang, *Adv Mater*, 2012, **24**, 4761-4764.
20. A. S. Ichimura, B. M. Mack, S. M. Usmani and D. G. Mars, *Chem Mater*, 2012, **24**, 2324-2329.
21. M. H. Jung, M. J. Chu and M. G. Kang, *Chem Commun*, 2012, **48**, 5016-5018.
22. W. J. Lee and Y. M. Sung, *Cryst Growth Des*, 2012, **12**, 5792-5795.
23. B. Liu and E. S. Aydil, *Chem Commun*, 2011, **47**, 9507-9509.
24. X. W. Wang, G. Liu, L. Z. Wang, J. A. Pan, G. Q. Lu and H. M. Cheng, *J Mater Chem*, 2011, **21**, 869-873.
25. H. Z. Yao, J. W. Ma, Y. N. Mu, Y. L. Chen, S. Su, P. Lv, X. L. Zhang, D. Ding, W. Y. Fu and H. B. Yang, *Rsc Adv*, 2015, **5**, 6429-6436.
26. S. J. Ding, J. S. Chen, D. Y. Luan, F. Y. C. Boey, S. Madhavi and X. W. Lou, *Chem Commun*, 2011, **47**, 5780-5782.
27. D. H. Wang, J. Liu, Q. S. Huo, Z. M. Nie, W. G. Lu, R. E. Williford and Y. B. Jiang, *J Am Chem Soc*, 2006, **128**, 13670-13671.
28. T. Sun, Y. Wang, M. Al-Mamun, H. Zhang, P. Liu and H. Zhao, *Rsc Adv*, 2015, **5**, 12860-12865.
29. H. M. Zhang, H. J. Zhao, S. Q. Zhang and X. Quan, *Chemphyschem*, 2008, **9**, 117-123.

30. H. M. Zhang, X. L. Liu, Y. B. Li, Q. F. Sun, Y. Wang, B. J. Wood, P. R. Liu, D. J. Yang and H. J. Zhao, *J Mater Chem*, 2012, **22**, 2465-2472.
31. H. M. Zhang, X. L. Liu, Y. Wang, P. R. Liu, W. P. Cai, G. S. Zhu, H. G. Yang and H. J. Zhao, *J Mater Chem A*, 2013, **1**, 2646-2652.
32. W. Wen, H. J. Zhao, S. Q. Zhang and V. Pires, *J Phys Chem C*, 2008, **112**, 3875-3880.
33. X. G. Han, Q. Kuang, M. S. Jin, Z. X. Xie and L. S. Zheng, *J Am Chem Soc*, 2009, **131**, 3152-+.
34. M. Kong, Y. Z. Li, X. Chen, T. T. Tian, P. F. Fang, F. Zheng and X. J. Zhao, *J Am Chem Soc*, 2011, **133**, 16414-16417.
35. K. L. Lv, Q. J. Xiang and J. G. Yu, *Appl Catal B-Environ*, 2011, **104**, 275-281.
36. Z. C. Lai, F. Peng, Y. Wang, H. J. Wang, H. Yu, P. R. Liu and H. J. Zhao, *J Mater Chem*, 2012, **22**, 23906-23912.
37. T. R. Gordon, M. Cargnello, T. Paik, F. Mangolini, R. T. Weber, P. Fornasiero and C. B. Murray, *J Am Chem Soc*, 2012, **134**, 6751-6761.
38. J. H. Pan, X. W. Zhang, A. J. Du, D. D. Sun and J. O. Leckie, *J Am Chem Soc*, 2008, **130**, 11256-11257.
39. H. G. Yang, G. Liu, S. Z. Qiao, C. H. Sun, Y. G. Jin, S. C. Smith, J. Zou, H. M. Cheng and G. Q. Lu, *J Am Chem Soc*, 2009, **131**, 4078-4083.
40. H. J. Zhao, Y. M. Shen, S. Q. Zhang and H. M. Zhang, *Langmuir*, 2009, **25**, 11032-11037.